Institut für Numerische Simulation
Rheinische Friedrich-Wilhelms-Universität Bonn
Wegelerstraße 6 • 53115 Bonn • Germany
phone +49 228 73-3427 • fax +49 228 73-7527
www.ins.uni-bonn.de

P. Diehl, M. A. Schweitzer

Simulation of wave propagation and impact damage in brittle materials using peridynamics

INS Preprint No. 1628

December 2016

Simulation of wave propagation and impact damage in brittle materials using peridynamics

Patrick Diehl and Marc Alexander Schweitzer

Abstract

In this paper we present the results of simulating wave propagation and impact damage in brittle materials, like ceramics, using peridynamics, a non-local generalization of continuum mechanics. Two different bond-based material models, the prototype microelastic material model and its improved version, were used to model aluminum oxynitride (ALON). To validate the simulations, the speed of the wave front is compared with measured data of the edge-on impact (EOI) experiment. The presented simulation results indicate that convergence is attained, however, a modeling error of 10% remains. Which indicates that simple bond-based peridynamics models may not be sufficient to achieve sufficient accuracy in these applications, but more sophisticated state-based peridynamics models must be employed.

Key words: Wave propagation and impact damage; Peridynamics; Edge-On Impact experiment.

Patrick Diehl
Patrick Diehl, Institute for Numerical Simulation, Wegelerstr. 6, 53115 Bonn, e-mail: diehl@ins.uni-bonn.de

Marc Alexander Schweitzer
Marc Alexander Schweitzer, Institute for Numerical Simulation, Wegelerstr. 6, 53115 Bonn, e-mail: schweitzer@ins.uni-bonn.de

1 Introduction

Ceramic materials are of great relevance in industry. For instance, ceramics are an essential ingredient of batteries in electric/hybrid cars or modern airplanes. An important feature of this kind of battery is the safety of the ceramic core during a crash or accident. To this end, the precise approximation of the evolution of the damage and wave propagation in ceramics is highly important to ensure safe operation of such devices. A classical benchmark for impact damage in ceramic materials is the edge-on impact (EOI) experiment [16, 11, 19] developed in the 1980s for the visualization of wave propagation and impact damage.

Different macroscopic ceramic models were used to simulate this experiment as a benchmark against experimental data. One is the Kayenta material model [3], which is a generalized plasticity model for ceramics. Employing this material model in a traditional mesh-based discretization on a Lagrangian hexahedral mesh, yields an average of 83% of damage velocity of the experimental results, but damage and the resulting cracks align in a preferential horizontal and vertical fashion [8]. Thus, the common problem of mesh-alignment is observed. With traditional particle-based methods like smoothed-particle hydrodynamics (SPH), however, damage and cracks are usually smeared out [10, 1]. Thus, no satisfactory simulation approach is currently available for these applications.

We apply the bond-based peridynamics [12, 9], a non-local generalization of continuum mechanics, with focus on discontinuous solutions as they arise in fracture mechanics. The so-called EMU-peridynamics, a particle-based discretization approach can be classified as a total-Lagrangian collocation method with nodal integration. Here no mesh is involved and the alignment of cracks and fractures are not restricted to any mesh (similar to SPH). Peridynamics, however, allows for non-smooth kernel functions and with the EMU discretization modeling of local damage is possible. Thus, we hope to overcome the deficiencies of SPH and attain more accurate and reliable results.

To describe brittle material like ceramics we use the prototype microelastic brittle (PMB) model [13] and its improved version [7] as constitutive material laws. These bond-based material models include a notion of failure, but are applicable only to "Cauchy crystals" where $\nu = 1/4$. The "free" material parameters of both models can be obtained from the bulk modulus and the critical stress intensity factor of classical elasticity theory.

The remainder of this paper is structured as follows: In section 2 we shortly present the simple bond-based peridynamics (PD), whose discrete structure is computationally similar to SPH or molecular dynamics (MD). Here the employed constitutive law, the prototype microelastic brittle Material (PMB) model, is introduced. Section 3 presents the improvements to the EMU discretized version of the PMB model, the conversion of the classical materials parameters of elasticity theory to the employed PD constitutive material model and a comparison of these two models. In section 4 the model problem, the edge-on impact (EOI) experiment, is briefly introduced and the damage velocity extracted from the simulations is compared with the experimental data provided in [17, 18]. Finally, we conclude with a compari-

son of the two material models and discuss the issues of the macroscopic models of [3, 10, 1] with respect to the presented bond-based peridynamics.

2 Peridynamics

In this paper we use simple bond-based peridynamics (PD) [12], a non-local generalization of continuum mechanics, with a focus on discontinuous solutions as they arise in fracture mechanics. Peridynamics models dynamic cracks and fractures on a mesocopic scale. The principle of the theory is, that a particle at position x interacts with all other particles x' inside a finite interaction zone $B_\delta(x)$ by exchanging forces.

For introducing peridynamics, its discretization and the employed material models we use the following notation: We denote the set of particles (discretization points) as $P := \{p_i | i = 1,\dots,n\}$ with initial positions $X := \{x_i | i = 1,\dots,n\}$ in the reference configuration $\mathscr{R}$ and assign to each particle a the surrounding volume fragment V_j. The positions of the particles P in the deformed material configuration $Y_t = \{y_i | i = 1,\dots,n\}$ at time t are obtained by $y_i(t) := x_i + u(x_i,t)$. Assuming all particles P are placed at the nodes of regular grid, we can define $dx := ||x_j - x_i||$ as the discrete particle spacing. The displacement field u is given by the PD equation of motion

$$\rho(x)\ddot{u}(x,t) = \int_{B_\delta(x)} f(u(x',t) - u(x,t), x' - x)dx' + b(x,t), \tag{1}$$

with mass density $\rho(x)$, f as the kernel function, modeling the interaction of particles x and x' in the initial reference configuration and $b(x,t)$ denotes the external force. Here $B_\delta(x)$ denotes the finite interaction zone of the particle at position x with the cut-off radius δ, see Figure 1. Discretizing Equation (1) in space by a colloca-

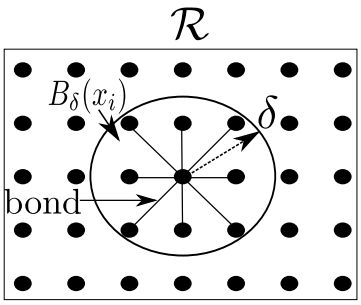

Fig. 1 Shows the reference configuration $\mathscr{R}$ of the particles $P := \{p_i | i = 1,\dots,n\}$ with initial positions $X := \{x_i | i = 1,\dots,n\}$. All particles inside the interaction zone $B_\delta(x_i)$ of the particle x_i are connected by bonds to exchange forces.

tion approach, the standard discretization for bond-based PD, using particles P and initial positions X yields

$$\rho(x_i)\ddot{u}(x_i,t) = \sum_{j\in\mathscr{F}_i} f(u(x_j,t)-u(x_i,t),x_j-x_i)\tilde{V}_j + b(x_i,t), \tag{2}$$

with $\tilde{V}_j := |V_j \cap B_\delta(x_i)|$. The interaction zone $B_\delta(x_i)$ in the discrete setting is given by the set $\mathscr{F}_i = \left\{ j \,|\, ||x_j - x_i|| \leq \delta, i \neq j \right\}$. This set depends only on the initial positions X, see Figure 1. All particles inside the set $\mathscr{F}_i$ are connected with so–called bonds. Equation (2) describes the general principle of the interaction between particles, but gives no explicit information about the behavior of the material. All information about the material and the constitutive material law is hidden in the kernel function f. For more details see [9, 13]. In the next subsection the prototype micro elastic brittle (PMB) material model is presented to describe the behavior of brittle materials, like aluminiumoxynitrid (ALON).

2.1 Prototype microelastic brittle material model

The prototype microelastic brittle (PMB) model was introduced in [13] as a nonlinear microelastic material model with a notion of failure. Let us shortly introduce this model. To this end, we define the relative position of two particles p and p' in the reference configuration as $\xi := x' - x$ and their relative displacement as $\eta(t) := u(x',t) - u(x,t)$. So the current relative position is $\xi + \eta(t)$. In the following we drop the time t and simply refer to $\eta(t)$ by η.

In the PMB model we assume, that the pairwise force function f, which models internal forces, depends only on the relative normalized bond stretch

$$s(\xi,\eta) := \frac{||\xi+\eta|| - ||\xi||}{||\xi||}. \tag{3}$$

For a bond under tension the function s obviously attains positive values.[1] The pairwise force function in the PMB material model is defined as

$$f(\xi,\eta,t) := c \cdot s(\xi,\eta,t) \cdot \mu(\xi,\eta,t) \frac{\xi+\eta}{||\xi+\eta||}, \tag{4}$$

with the material dependent stiffness constant c, s the bond stretch (3) and μ denoting a scalar valued history dependent function to model damage. To this end, the function

$$\mu(\xi,\eta,t) = \begin{cases} 1 & s(\xi,\eta,t) < s_c - \alpha s_{\min}(t'), \forall 0 \leq t' \leq t, \\ 0 & otherwise. \end{cases} \tag{5}$$

[1] Note that we assume isotropic material behavior due to the fact that s depends on $||\xi||$.

indicates if a bond is broken. Here, denotes s_c the critical bond stretch for bond failure in a particular material and $s_{\min}(t') := \min_{\xi} s(\xi, \eta, t')$. The parameter α is usually fixed at 0.25 [13]. The influence of this parameter on the material behavior has been studied in [6] and with respect to this study we fixed the parameter α to the suggested value of 0.25. Figure 2 shows the plot of the pairwise bond force f as

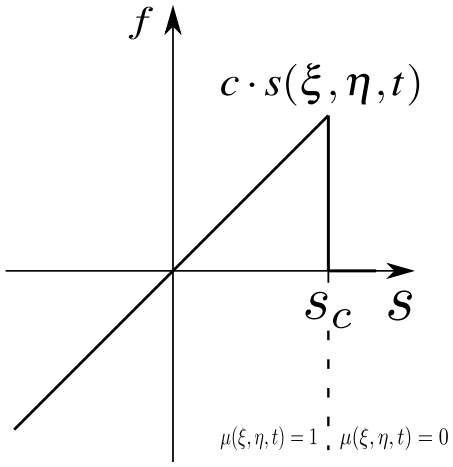

Fig. 2 Plot of the pairwise bond force f as a linear valued function with the stiffness constant c as slope and the critical bond stretch for bond failure s_c as the decrease to zero.

a function of the bond stretch s. This function is linear with the stiffness constant c as slope and drops to zero for $s > s_c$, which means that the bond between these two particles is broken. To attain in the continuum model conservation of linear momentum f must satisfy $f(-\xi, -\eta) = -f(\xi, \eta)\ \forall \eta, \xi$ and hold to attain the conservation of angular momentum $(\eta + \xi) \times f(\xi, \eta) = 0\ \forall \eta, \xi$.

Thus, the stiffness constant c and the critical bond stretch for failure s_c are the only material dependent parameters in the PMB model. The next step is to obtain these parameters from well-known material parameters of classical elasticity.

To this end, we assume that a microelastic material is derivable from a scalar micro potential ω

$$f(\xi, \eta) = f(x' - x, \eta) = \frac{\partial \omega}{\partial \eta}(x' - x, \eta)\ \forall \eta, \xi = x' - x. \tag{6}$$

This gives the energy of a single bond and the total strain energy density W_{PD} of all bonds in $B_\delta(x)$ is obtained by

$$W_{\mathrm{PD}} = \frac{1}{2} \int_{B_\delta(x)} \omega(x' - x, \eta) dx'. \tag{7}$$

Assuming $\omega = 1/2cs^2\xi$ is a valid micro potential for a large homogeneous body under isotropic tension and applying (7) yields

$$W_{\text{PD}} = \int_0^\delta \frac{1}{4} cs^2 \xi^2 dx' = \frac{1}{4}\pi cs^2\delta^4. \tag{8}$$

To obtain the stiffness constant c, we assume, that the energy density W_{PD} is equivalent to the classical strain energy density $W = 9Ks^2/2\,\text{N}\,\text{mm}^{-2}$ of classical elasticity for this material. Such that the energy for the deformation in the PMB model is the same as the energy for the same deformation in classical elasticity. This energy equivalence delivers

$$\frac{1}{4}\pi cs^2\delta^4 \;=\; \frac{9}{2}Ks^2 \Rightarrow c(K,\delta) = \frac{18K}{\pi\delta^4}. \tag{9}$$

With this energy equivalence the stiffness constant $c(K,\delta)$ depends on the bulk modulus K a material parameter and the horizon δ, a discretization parameter.

To obtain the critical stretch for bond failure s_c we consider a large homogeneous body and the energy to break the body (i.e. $B_\delta(x)$) vertically into two halves U_δ and L_δ. Thus, the bonds of all particles in U_δ to any particle in L_δ must be stretched beyond the critical value s_c.

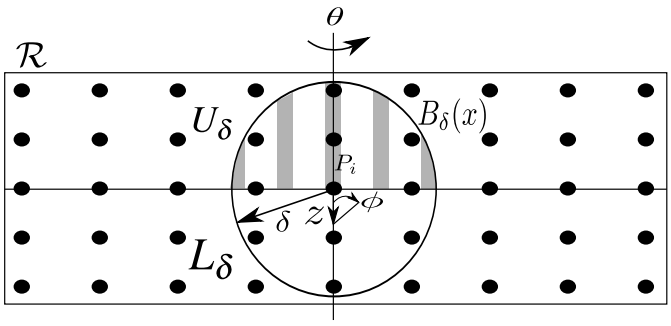

Fig. 3 The body $\mathscr{R}$ in the reference configuration vertically divided in U_δ and L_δ. To obtain the critical stretch for bond failure s_c the energy to break all bonds of particles along z to particles inside the interaction zone $B_{\delta(x_i)}$ in the other half is estimated.

Figure 3 shows the body $\mathscr{R}$ in the reference configuration divided into U_δ and L_δ. To compute the total energy to break all bonds connected to particles in the other half, we first need to consider all particles along the z-direction, this yields the first integral in Equation (10).

$$G_{\mathrm{PD}} = \int_0^{\delta}\int_0^{\delta}\int_0^{2\pi}\int_0^{\arccos\left(\frac{z}{\xi}\right)} 1/2cs^2\xi^2 \sin\phi d\theta d\phi d\xi dz = \frac{\pi c s_c^2 \delta^5}{10} \tag{10}$$

The second integral is the integration over U_δ, the third one is the rotation with the angle θ and the last one the condition, that only particles connected in the reference configuration $\mathscr{R}$ are connected with bonds. To obtain the critical bond stretch for failure Equation (10) is solved for s_c which gives

$$s_c = \sqrt{\frac{10G_{\mathrm{PD}}}{\pi c\delta^5}} \overset{(9)}{=} \sqrt{\frac{10G_{\mathrm{PD}}\pi\delta^4}{\pi 18K\delta^5}} = \sqrt{\frac{5G_{\mathrm{PD}}}{9K\delta}}. \tag{11}$$

Again, the energy G_{PD} is assumed to be equal to the energy release rate $G := K_{\mathrm{Ic}}^2(1-\nu^2)/E$ of classical elasticity theory with $\nu = 1/4$ and the Young modulus $E = 3K(1-2\nu)$. Thus, that we end up with

$$s_c(K, K_{\mathrm{Ic}}, \delta) = \frac{5}{12}\sqrt{2}\sqrt{\frac{K_{\mathrm{Ic}}^2}{K^2\delta}}. \tag{12}$$

Note, that in the continuum model (1) we integrate over the interaction zone $B_\delta(x)$ and assume that each particle x' has the same influence independent on the the distance to the cut-off radius. In the discrete model in Equation (2) the volume V_j of the particle p_j is $\tilde{V}_j = |V_j \cap B_\delta(x_i)|$, such that particles x' further away from x have less influence. In a computational point of view a expensive intersect operation is applied to compensate the over prediction in the continuum model.

3 Improved prototype microelastic brittle material model

Here the PMB model is adjusted to the EMU discretization method, because it is assumed that all particles P have the same surrounding volume V. Thus, all particles have the same stiffness constant c and the same critical failure for bond stretch s_c. For non-homogeneous materials or modeling material defects, a non-uniform spatial partitioning is preferable. Then, that each particle p_i has its own stiffness constant $\overline{c_i}$ and critical bond stretch for failure $\overline{s}_{c_i}$, depending on the interaction zone $\mathscr{F}_i$. In [7] a normalization of the PMB model is suggested to obtain the stiffness constant $\overline{c}_i$ and the critical bond stretch for failure $\overline{s}_{c_i}$. Here, some experiments with sound wave propagation shows that the PMB model over-predict the speed of sound by 13%. The improved model agrees with the theoretical result with an error of 1%. Thus, we want to look at the improvements of this model and employ it also in our benchmark. Note, that in [7] the computation for the critical bond stretch for failure $\overline{s}_c$ is only presented for two dimensional case.

In the original PMB model, described in section 2.1, the stiffness constant is derived from an analytic solution of the integral (8). In the discrete EMU setting the

integral is approximated via a summation over the particles in $\mathscr{F}_i$, the same way as in Equation (2), which yields

$$\frac{1}{2}\int_{B_\delta(x)} \overline{\omega}(\xi,\eta)dx' \approx \frac{1}{2}\sum_{j\in\mathscr{F}_i} \overline{\omega}(\xi,\eta)V_j. \tag{13}$$

In the discrete version of the improved PMB model the symmetry of the pairwise force function $\overline{f}(-\xi,-\eta) = -\overline{f}(\xi,\eta)$ does not hold necessarily, since the overall volume of all particles in the interaction zone $B_\delta(x)$ can differ, due to the fact that particles can have different volumes. We define the potential $\overline{\omega}(\xi,\eta) = (w_{i,j}\overline{c}\overline{s}_{ij}^2)/2$ with the weights $w_{ij} = 1\,\forall i,j$ and $\bar{s}_{ij} = s\,\forall i,j$, so that the sum over all bonds is the overall stretch s yields

$$\frac{1}{2}\sum_{j\in\mathscr{F}_i} \overline{\omega}(\xi,\eta)V_j = \frac{1}{2}\sum_{j\in\mathscr{F}_i}\frac{1}{2}w_{i,j}\overline{c}\overline{s}_{ij}^2V_j = \frac{1}{4}\sum_{j\in\mathscr{F}_i}\bar{c}s^2V_j. \tag{14}$$

Here the energy equivalence for the strain energy density $\overline{W} = \frac{9}{4}Ks^2$ in two dimensions is used, such that

$$\frac{1}{4}\sum_{j\in\mathscr{F}_i}\bar{c}s^2V_j = \frac{9}{4}Ks^2 \Rightarrow \bar{c}_i(K,dx) = \frac{9K}{\sum\limits_{j\in\mathscr{F}_i}V_j}. \tag{15}$$

Due to the assumption that the volume of the interaction zone $B_\delta(x)$ of each particle p_i can differ, each particle has its own stiffness constant $\bar{c}_i$. It depends on the bulk modulus K and only differs in the volume of the interaction zone.

For the critical bond stretch for failure $\bar{s}_{c_i}$ we look at the two dimensional plane, see Figure 4, and assume, that the energy release rate $\overline{G}_{\mathrm{PD}}$ is obtained by the integration of the energy density $\overline{\omega}(\eta,\xi)\overline{V}(h,\delta)$ over all fracture planes with the heights h. The volume of a fracture plane $\overline{V}(h,\delta)$ is the thickness t of the plane multiplied by the area of the circular segment $\delta^2\arccos(\frac{\delta-h}{\delta}) - (\delta-h)\sqrt{2\delta h - h^2}$. These assumptions yield

$$\overline{G}_{\mathrm{PD}} = 2\overline{\omega}(\eta,\xi)\int_0^\delta \overline{V}(h,\delta)dh = \frac{2}{3}\bar{c}\bar{s}^2t\delta^3. \tag{16}$$

Note, that in the discrete model each particle p has a own stiffness constant and $\bar{c}_i \neq \bar{c}_j$, to enforce symmetry, due to conversation of linear momentum, we introduce the average $\bar{c}_{ij} = (\bar{c}_i + \bar{c}_j)/2$.

Here the same energy equivalence as in the PMB model is used to obtain the energy release rate $\overline{G}_{\mathrm{PD}}$ from values of the classical elasticity theory

$$\frac{2}{3}\bar{c}_{i,j}\bar{s}^2t\delta^3 = \frac{5K_{\mathrm{Ic}}^2}{8K} \Rightarrow \bar{s}_{\bar{c}_{ij}}(K,K_{\mathrm{Ic}},\delta,t) = \frac{1}{4}\sqrt{15}\frac{K_{\mathrm{Ic}}}{\sqrt{K\bar{c}_{i,j}t\delta\delta}} \tag{17}$$

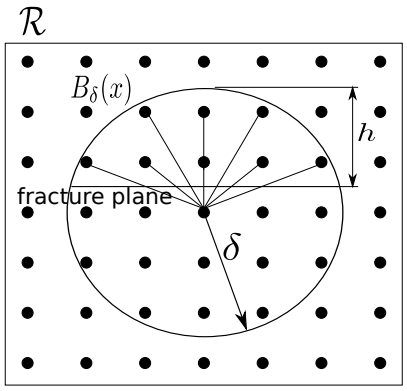

Fig. 4 To obtain the fracture energy we look at the neighborhood $B_\delta(x_i)$ of an particle p_i. To obtain the energy release rate $\overline{G}_{\mathrm{PD}}$ the energy density is integrated over the interaction zone $B_\delta(x)$ by varying the height h of the fracture plane.

Note, that in this discrete model each particle p_i has its own stiffness constant $\overline{c}_i$ and critical bond stretch for failure $\overline{s}_{c_{ij}}$ derived from the classical material parameters as in the original model, however, accounting for numerical integration errors.

3.1 Comparison of the material models

Table 1 gives an overview of the material parameters in the two different material models. The stiffness constant depends in both materials on the bulk modulus K and

Table 1 Overview of the two material parameters in the two different models.

Model	stiffness constant c	critical bond stretch for failure s_c
PMB	$c(K,\delta) = \dfrac{18K}{\pi\delta^4}$	$s_c(K,K_{\mathrm{Ic}},\delta) = \dfrac{5}{12}\sqrt{2}\sqrt{\dfrac{K_{\mathrm{Ic}}^2}{K^2\delta}}$
Normalized PMB	$\overline{c}_i(K,dx) = \dfrac{9K}{\sum\limits_{j\in\mathcal{F}_i} V_j}$	$\overline{s}_{\overline{c}_{ij}}(K,K_{\mathrm{Ic}},\delta,t) = \dfrac{1}{4}\sqrt{15}\dfrac{K_{\mathrm{Ic}}}{\sqrt{K\overline{c}_{i,j}t\delta\delta}}$

the discretization parameter dx. The critical bond stretch for failure depends with respect to the materials parameters ancillary on the critical stress intensity factor K_{Ic}. Note, that in the normalized PMB model the thickness of the geometry t is added as a further parameter. In [13] the assembly of the particles as the nodes of a regular grid with the lattice constant dx and a horizon $\delta = 3dx$ is suggested.

According to the assembly on a regular grid the volume of an particle p_i is chosen as $V_i = dx^3$. Figure 5 shows the dependency of the material parameters with respect to the lattice constant dx and a constant bulk modulus $K = 210 \times 10^9$ Pa and critical stress intensity factor K_{Ic}=2×10^6 Pa$\sqrt{\text{m}}$, which are common values for ALON. The

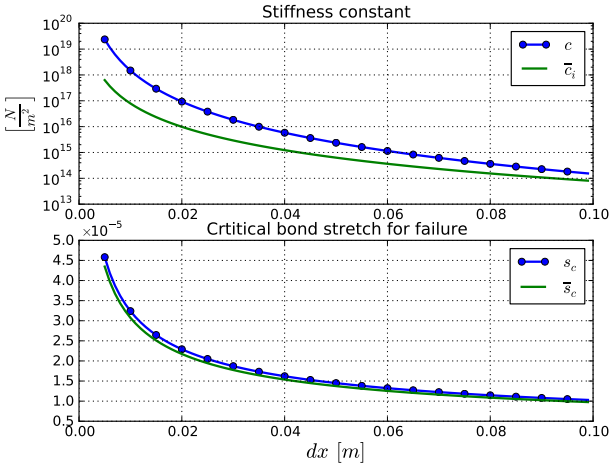

Fig. 5 Plot of the two material constants with respect to the lattice constant dx for ALON with common values for the bulk modulus $K = 210 \times 10^9$ Pa and critical stress intensity factor $K_{\text{Ic}} = 2 \times 10^6$ Pa$\sqrt{\text{m}}$.

stiffness constant differs by two orders of the magnitude and the critical stretch for bond failure differs marginal.

4 Numerical Results

In this chapter we compare the results for our bond-based peridynamics simulations with the experimental data from [17, 18]. The initial positions X are the nodes of a uniform grid with mesh-width $dx = dy = dz$. As the cut-off radius δ of the interaction zone $B_\delta(x_i)$ we choose $\delta = 3dx$, as suggested in [13].

Note, that we used a single GPU-based implementation of peridynamics [4] for the simulations and we are therefore restricted to the memory limitations of the Nvidia Tesla M2090 GPU with 6GB memory. Due to the computationally expensive improvements of the PMB model, e.g storing two additional constant for each particle, the number of particles that can be used in the simulations with the improved model is (substantially) smaller for the PMB model.

As indicated by the sketch given in Figure 6, there are various convergence scenarios considered in PD [5]. The most common limit $u_{0,0}$ considered is $\delta =$

$3dx, dx \to 0$. In our study we consider additionally the limit $u_{\delta,0}$ for $\delta = \text{const}, dx \to 0$ and the limit $u_{0,dx}$ for $\delta \to 0, dx = \text{const}$.

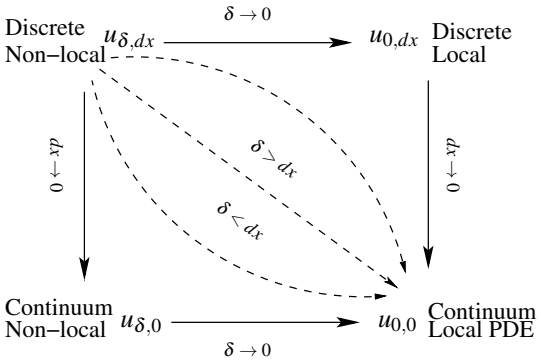

Fig. 6 Various convergence issues and limits as $\delta, h \to 0$.

4.1 Model problem: Edge-On Impact experiment

The edge-on impact (EOI) experiment was developed by the Ernst-Mach-Institute to visualize dynamic fracture in brittle materials using the high-speed photographic technique [16]. First tests with a glass plate were completed in the late 1930s [11]. In the 1980s this technique was rediscovered to visualize impact damage and wave propagation in ceramic materials [19]. This experimental data obtained in [16] was moreover used as a benchmark for the Kayenta model [3, 8] and SPH with a Lagrangian hydrocode approach [10]. Thus, we use this experiment as a benchmark for the bond-based peridynamics for wave propagation and impact damage and compare our simulations results with the Kayenta model and SPH.

Let us shortly summarize the simulation setup. For detailed information, especially for the visualization of the wave propagation, see [11, 16]. We used the experiments, described in [17, 18] to compare our simulation results with experimental data. Figure 7(a) shows the experimental assembly and Figure 7(b) the dimensions of the steel projectile and the ALON specimen. Table 2 shows the measured wave velocities at a nominal impact velocity of 380 $\mathrm{m\,s^{-1}}$.

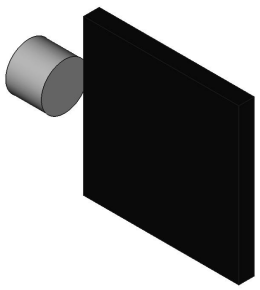

(a) Experimental assembly.

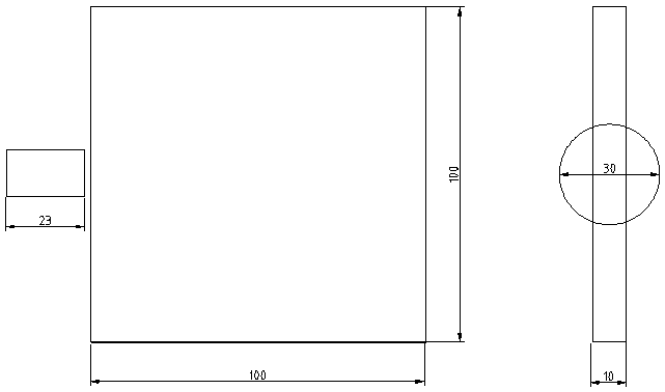

(b) Blueprint of the projectile and specimen.

Fig. 7 The experimental assembly (a) of the experiment with a steel projectile and a specimen of aluminiumoxynitrid (ALON). The blueprint (b) shows the measurements of the projectile, a cylinder with the diameter of 30 mm and a length of 23 mm, and the specimen $(100\text{ mm}\times 100\text{ mm}\times 10\text{ mm})$. The force $b(x_i,t)$ the indenter exerts to the plate is 3.8×10^5N.

4.2 Comparison of Results

Here we compare the obtained speed at the wave front with the experiments in [17, 18]. Figure 8-10 show the speed of the wave front and the speed of the coherent damage front obtained for a nominal velocity of 380 $\text{m}\,\text{s}^{-1}$ at time 8.7 µs (Table 2) and the resulting wave speed from the simulations for each limiting process described in Figure 6.

Table 2 Measured wave velocities for aluminum oxynitride (ALON) at a nominal impact velocity of 380 $\mathrm{m\,s^{-1}}$ at time 8.7 µs [17, 18].

Wave	Velocity $[\mathrm{m\,s^{-1}}]$
Wave front	9367
Coherent damage/fracture front	8381

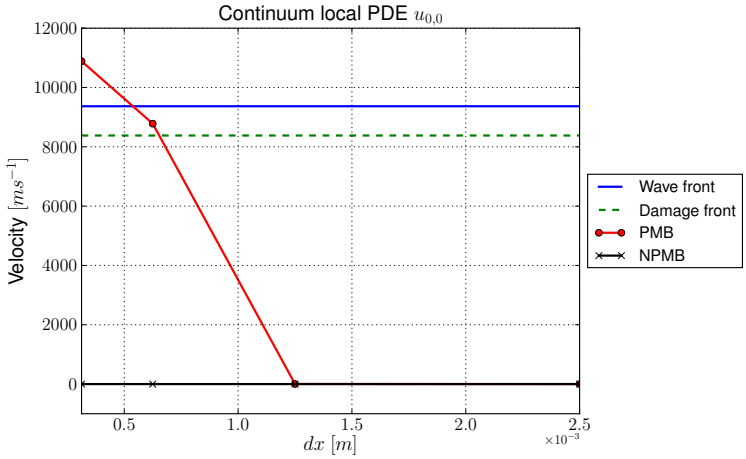

Fig. 8 Measured velocity of the wave front for the continuum local PDE $u_{0,0}$ limit. Here both parameters dx and $\delta = 3dx$ decreases to zero.

Figure 8 shows the results for the continuum local PDE $u_{0,0}$ limit. For this process both parameter $\delta = 3dx$ and dx go to zero. For the PMB model the propagation of the wave starts with decreasing dx. The obtained wave speed is close to the speed at the experimental damage front, but overshoots the experimental value for the speed at the wave front for the next dx. For the NPMB model we can not obtain the front wave in our simulations with the fitted parameter for $\delta = 3dx$ and the initial displacement of the particles as suggested in [9].

Figure 9 shows the results for the continuum local $u_{\delta,0}$ limit, here for both bond-based peridynamic materials models no wave propagation is obtained. In this setting $\delta = 3\max(dx)$ is fixed and for decreasing values of dx the maximal amount of neighbors $|\mathscr{F}_i|$ grows up to 1972. Thus, the interaction zone of the particle is too wide and the locality of the wave propagation can not be resolved. In [2] the suggested that smaller horizons get better results, since wave dispersion due to the size of the non-locality is reduced as the horizon decrease.

Figure 10 shows the discrete local limit where $dx = \min(dx)$ is fixed and the horizon delta is varied. We used the suggested $\delta = 3dx$ in [13] and decrease it to $2dx$, because for a horizon $\delta = dx$ the interaction zone is too small and crack and fracture align between the initial positions X of the particles. Thus, we have the same limitations as a mesh-based approach. Here for PMB we get the best result,

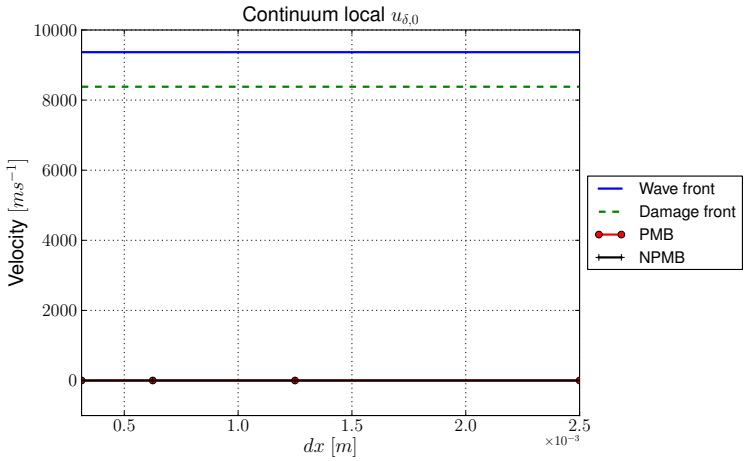

Fig. 9 Measured velocity of the wave front for the continuum local $u_{\delta,0}$ limit. Here $\delta = \text{const}$ is fixed and dx decreases to zero.

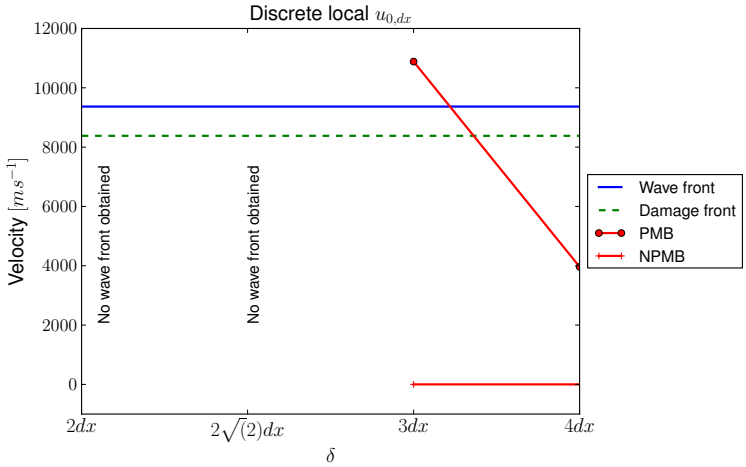

Fig. 10 Measured velocity of the wave front for the discrete local $u_{0,dx}$ limit. Here dx is fixed and $\delta \to dx$. Note, that for $\delta < dx$ an empty interaction zone $\mathscr{F}_i$ is attained.

as suggested in [14], to adjust the horizon so that the peridynamic results produce the same dispersion curves as those measured for a specific material. For the NPMB material model we used the same adjusted horizon and can not obtain the wave propagation process. Thus, the horizon should be adjusted for the NPMB model to reproduce the dispersion curves to get reliable results.

5 Conclusion and Outlook

We present the simulation of wave propagation and impact damage with two bond-based peridynamic materials model. As the reference we used the experimental values for the speed at the wave front and the coherent damage front in [17, 18]. For the prototype microelastic material model we obtain, that for the suggested horizon $\delta = 3dx$ in [13] the wave propagation is applicable. One reason is, that the horizon is adjusted for this model to reproduce the same dispersion curves as those measured for a specific material [14]. For the discrete local $u_{0,dx}$ limit (Figure 10), we see the effect, that smaller horizons get better results, since wave dispersion due to the size of the non-locality is reduced as the horizon decrease [2].

The improvements to the discrete model agree better to the theoretical results for sound wave propagation [7]. The results consider one idealized material, with a material density $\rho = 1\text{kg}/\text{m}^3$ and a bulk modulus $K = 1\text{Pa}$. For the simulation of wave propagation and impact damage we see no effect of these improvements to the discrete model. To get reliable results, the horizon δ should be adjusted as in [14].

The alignment of the damage and cracks in a horizontal and vertical fashion [3] is not observed for the PMB model. Due to the non-smooth kernel functions the crack and fractures locally develop for a "good" choice of the horizon δ, and do not smear out, like in other particle methods, like SPH [10]. Thus, simple bond-based peridynamics is applicable to simulate wave propagation and impact damage, but the adjustment of the horizon is very important for reliable results.

To achieve sufficient accuracy the more sophisticated state-based peridynamics [15] must be employed.

References

1. Benson, D.J.: Computational methods in lagrangian and eulerian hydrocodes. Computer Methods in Applied Mechanics and Engineering **99**(23), 235 – 394 (1992)
2. Bobaru, F., Hu, W.: The meaning, selection, and use of the peridynamic horizon and its relation to crack branching in brittle materials. International Journal of Fracture **176**(2), 215–222 (2012). DOI 10.1007/s10704-012-9725-z. URL
3. Brannon, R., Fossum, A., Strack, E.: Kayenta: Theory and User's Guide. Tech. Rep. SAND2009-2282, Sandia National Laboratories, Albuquerque (2009)
4. Diehl, P.: Implementierung eines Peridynamik-Verfahrens auf GPU. Diplomarbeit, Institute of Parallel and Distributed Systems, University of Stuttgart (2012)
5. Du, Q., Tian, X.: Robust discretization of nonlocal models related to peridynamics. In: M. Griebel, M.A. Schweitzer (eds.) Meshfree Methods for Partial Differential Equations VII, *Lecture Notes in Computational Science and Engineering*, vol. 100, pp. 97–113. Springer International Publishing (2015)
6. Franzelin, F., Diehl, P., Pflüger, D.: Non-intrusive uncertainty quantification with sparse grids for multivariate peridynamic simulations. In: M. Griebel, M.A. Schweitzer (eds.) Meshfree Methods for Partial Differential Equations VII, *Lecture Notes in Computational Science and Engineering*, vol. 100, pp. 115–143. Springer (2014)
7. Ganzenmüller, G.C., Hiermaier, S., May, M.: Improvements to the Prototype Micro-Brittle Linaear Elasticity Model of Peridynamics. In: M. Griebel, M.A. Schweitzer (eds.) Meshfree

Methods for Partial Differential Equations VII, *Lecture Notes in Computational Science and Engineering*, vol. 100, pp. 163–183. Springer (2014)
8. Leavy, R.B., Clayton, J.D., Strack, O.E., Brannon, R.M., Strassburger, E.: Edge on impact simulations and experiments. Procedia Engineering **58**(0), 445–452 (2013). Proceedings of the 12th Hypervelocity Impact Symposium
9. Parks, M.L., Lehoucq, R.B., Plimpton, S.J., Silling, S.A.: Implementing peridynamics within a molecular dynamics code. In: EL (ed.) Computer Physics Communications, vol. 179, pp. 777–783 (2008)
10. Riedel, W., Hiermaier, S., Thoma, K.: Transient stress and failure analysis of impact experiments with ceramics. In: Materials Science and Enginnering B, vol. 173, pp. 139–147. ELSEVIER (2010)
11. Schradin, H.: Physikalische Vorgänge bei hohen Belastungen und Belastungsgeschwindigkeiten (Physical Processes at High Loadings and Loading Rates). In: Scripts for German Academy for Aeronautical Research, vol. 40, pp. 21–68 (1939)
12. Silling, S.: Reformulation of elasticity theory for discontinuities and long-range forces. Journal of the Mechanics and Physics of Solids **48**(1), 175 – 209 (2000)
13. Silling, S., Askari, E.: A meshfree method based on the peridynamic model of solid mechanics. In: ELSEVIER (ed.) Computer & Structures, vol. 83, pp. 1526–1535 (2005)
14. Silling, S.A.: A coarsening method for linear peridynamics. Int. J. Multiscale Com. Eng. 9 **6**, 609–621 (2011)
15. Silling, S.A., Epton, M., Weckner, O., Xu, J., Askari, E.: Peridynamic States and Constititive Modeling. In: Journal of Elaasticity, vol. 88, pp. 151–184. Springer Science + Business Media B. V. (2007)
16. Strassburger, E.: Visualization of Impact Damage in Ceramics Using the Edge-On Impact Technique. In: International Journal of Applied Ceramic Technology, vol. 1, pp. 1:235–242 (2004)
17. Strassburger, E., Patel, P., McCauley, J.W., Tempelton, D.W.: Visualization of wave propagation and impact damage in a polycrystalline transparent ceramic - AlON. In: 22nd International Symposium on Ballistics, 2, pp. 769–776. DEStech Publications (2005)
18. Strassburger, E., Patel, P., McCauley, J.W., Templeton, D.W.: High-Speed Photographic Study Of Wave Propagation And Iimpact Damage In Fused Silcia And Alon Using The Edge-On Impact (EOI) Method. AIP Conf. Proc. **892** (2006). DOI http://dx.doi.org/10.1063/1.2263465
19. Winkler, S., Senf, H., Rothenhausler, H.: Wave and Fracture Phenomena in Impacted Ceramics. EMI-Report V5/89, FRAUNHOFER-INST fuer Werkstoffmechanik Freiburg (1989)